Langmuir

Article

pubs.acs.org/Langmuir

Defect-Mediated Formation of Ag Cluster-Doped TiO_2 Nanoparticles for Efficient Photodegradation of Pentachlorophenol

Hemin Zhang, Changhao Liang,* Jun Liu, Zhenfei Tian, Guozhong Wang, and Weiping Cai

Key Laboratory of Materials Physics and Anhui Key Laboratory of Nanomaterials and Nanotechnology, Institute of Solid State Physics, Hefei Institutes of Physical Science, Chinese Academy of Sciences, Hefei 230031, China

Supporting Information

ABSTRACT: A novel strategy was designed to prepare Ag cluster-doped TiO_2 nanoparticles (Ag/TiO_2 NPs) without addition of any chemical reducing agent and/or organic additive. A defect-rich TiO_x species was generated by laser ablation in liquid (LAL) of a Ti target. The silver ions could be reduced and deposited on the surface of TiO_2 NPs through the removal of oxygen vacancies and defects; the TiO_x species evolved into anatase NPs in a hydrothermal treatment process. The derived Ag/TiO_2 NPs are approximately 25 nm in size, with narrow size distribution. The Ag clusters are highly dispersed inside TiO_2 and less than 3 nm in size. The doped amount can be tuned by changing the concentration of Ag^+ ions. The as-synthesized Ag/TiO_2 NPs display improved photocatalytic efficiency toward pentachlorophenol (PCP) degradation.

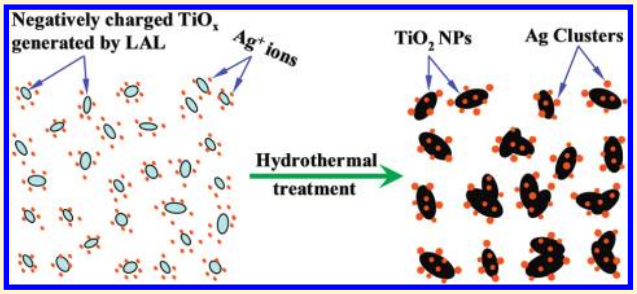

INTRODUCTION

Combinations of a catalytically active noble metal and a key semiconductor material have received much attention owing to their wide application in fields ranging from photochemistry to heterogeneous catalysis.[1−3] The size, dispersion, and amount of noble metal particle are key to the properties of metal/semiconductor composites.[4,5] Especially, the size of the metal particles can potentially modify the electronic properties of the composites. For example, Turner and co-workers[6] demonstrated that, when the sizes of metal particles fall below 2.0 nm, the composites would display unusual catalytic behavior. Light-excited semiconductor nanoparticles (NPs) coupling with noble metal NPs undergo charge equilibration and shift their Fermi level closer to the conduction band of the semiconductor,[4,7] thus improving their photocatalytic and photoelectrochemical responses by reducing the fast recombination of the photogenerated charge carriers.[8]

Among the various such nanocomposite structures, the well-known Ag/TiO_2 nanocomposite has attracted considerable interest for its application in fields including photocatalysis, energy conversion,[9] antibacterial activity,[10] and pollutant degradation[11,12] due to (1) TiO_2's chemical inertness, nontoxicity, and biological compatibility, and (2) Ag's bactericidal capability,[13] size- and shape-dependent optical properties,[14] and remarkably low human toxicity compared to other heavy metal ions.[15,16] Critically, silver composites occupy an exceptional position among metals as the work function of silver is much lower than that of other noble metals such as gold and platinum.[17]

Toward manipulating the particle size and dispersion of Ag, various methods have been attempted to fabricate Ag/TiO_2 nanocomposite. The most used method to obtain Ag NPs is the chemical reduction of Ag^+ ion in solution, which usually involves a reducing agent and a stabilizing additive. For example, a colloidal approach to Ag/TiO_2 nanocomposite involves admixture of organic-capped anatase TiO_2 solids obtained by hydrolysis of titanium tetra-isopropoxide using oleic acid as a surfactant with a very dilute solution of $AgNO_3$ in $CHCl_3$/EtOH.[18] In another route, addition of citrate ions (a reducing agent) to silver colloids results in the complexation of citrate with silver colloids, producing particles of various shapes and sizes (50−100 nm).[19] In the above methods, the organic ligands and/or chemical agents employed potentially affect the solid-state and optical properties of the particles;[18] furthermore, stabilizers can seriously influence catalytic activity, resulting in significant blockage of active sites.[20,21] Therefore, the implementation of a simple process to uniformly deposit Ag NPs onto TiO_2 without the use of organic surfactants and/or chemical reducing agents is important and also a great challenge.

To meet the above requirement, in this study, a new strategy combining laser ablation in liquid (LAL) technique and hydrothermal treatment was designed to obtain Ag cluster-doped TiO_2 NPs without using any chemical reducing agent and/or organic additive. Ag clusters with size less than 5 nm were highly dispersed onto surfaces of TiO_2 NPs. Many metal oxide species produced by LAL have metastable phase and/or unsaturated valences, with obvious oxygen vacancies.[22]

Received: November 5, 2011
Revised: January 30, 2012
Published: February 15, 2012

Scheme 1. Schematic Illustration for the Synthesis of Ag/TiO_2 NPs

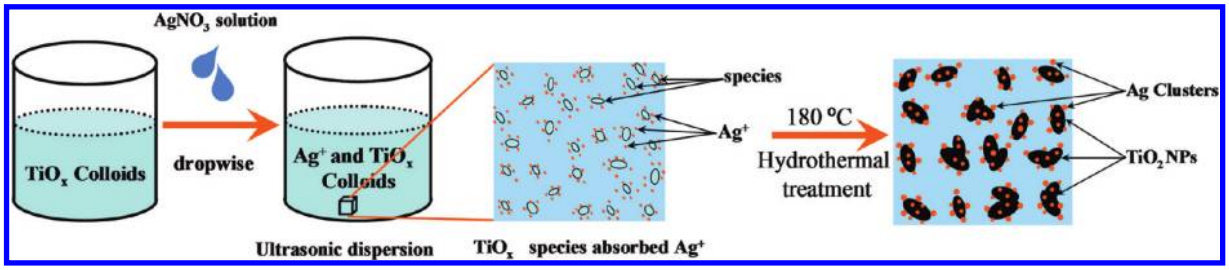

Resultantly, these metal oxide species usually possess weak reducibility and negatively charged surfaces, both of which are advantageous to the absorption and reduction of positively charged noble metal ions during further crystallization, ripening, and diminishing of oxygen vacancies in a hydrothermal treatment process.

EXPERIMENTAL DETAILS

Preparation of Ag/TiO_2 NPs. The Ag/TiO_2 NPs were first synthesized by hydrothermal treatment of the mixture of $AgNO_3$ solution and TiO_x colloids induced by LAL, a facile technique for ultrafine oxides NPs as previously described.[23,24] Briefly, a titanium target with 99.98% purity was first fixed on a supporter in a vessel filled with 20 mL of deionized water. While the target was being irradiated, the vessel was rotated (10 rpm) by a motorized tunable stage (WNSC 400). A Nd/YAG pulsed laser (1064 nm, 10 Hz, pulse duration of 8 ns, pulse energy of about 120 mJ, and spot size of 1.5 mm in diameter) was focused on the target for 20 min. Portions (40 mL) of LAL-derived colloids were mixed with 2.1 mL of $AgNO_3$ solution with concentrations of 0, 0.1, or 0.2 M. Subsequently, the colloidal suspensions were transferred to 60 mL Teflon-lined stainless steel autoclaves and kept in an electric oven at 180 °C for 24 h. After hydrothermal treatment, the solutions were centrifuged at 10 000 rpm; powderlike products were collected. The concentration of the doped Ag cluster was calculated to be approximately 0 atom %, 0.54 atom %, and 1.08 atom %, respectively, relative to TiO_2 in the final samples. The products were subject to three rounds of ultrasonic rinsing to obtain pure powders, which were then kept in a vacuum-drybox at 25 °C.

Characterization of Ag/TiO_2 NPs. The collected powder products were deposited onto a glass substrate for analysis by an X-ray diffractometer (XRD, Philips X'Pert) with Cu Kα radiation (λ = 0.15419 nm, scan step size = 0.033492°, and time per step = 200.025 s). Morphology and structure investigations were performed using transmission electron microscopy (TEM) with 200 kV acceleration voltages; the microscope (JEOL, JEM-2010) was equipped with an Oxford INCA energy-dispersive X-ray spectroscope for microscopic elemental analysis. The TEM specimens were prepared by dispersing the powders in ethanol to form suspensions, which were then dropped onto a carbon-coated Cu grid. X-ray photoelectron spectrum (XPS) analysis was performed using an Al Kα X-ray source on a Thermo-VG ESCALAB MKII spectrometer. The UV−vis spectra were collected using a Shimadzu UV-2550 spectrometer. Zeta potential was measured using a Zetasizer 3000 HSa. The residual concentration of silver ions was monitored by inductively coupled plasma spectroscopy (ICP, IRIS Intrepid II ICP-OES).

Photodegradation Tests. Pentachlorophenol (PCP), a commonly used industrial organic pollutant, was used as a model pollutant to test the photocatalytic properties of the Ag/TiO_2 NPs. A 20 mL PCP solution with an initial concentration of 20 mg L^{-1} in the presence of powder catalyst (2.5 mg) was illuminated under UV light (UV-A, 365 nm). The solutions were continuously stirred in the dark for 20 min to achieve adsorption−desorption equilibrium. Before light irradiation, powder catalysts were added to three chambers with PCP solution. The distance between the UV light source and the chambers was about 10 cm. The time-dependent concentration change of PCP remaining in the solution was monitored using a UV−vis spectrometer at 213 nm.

RESULTS AND DISCUSSIONS

Formation Process of Ag/TiO_2 NPs. Successful synthesis of Ag cluster-doped TiO_2 NPs was based on distinctive properties of the colloids induced by LAL, involving ultrasmall size, amorphous and noncrystalline, incomplete oxidation, and rich defects. As shown in Scheme 1, the synthesis starts with a colloidal suspension obtained by LAL using the rotated Ti target, which contains a large amount of homogeneously dispersed species of TiO_x ($x \approx 1.4$). Definitely, these species are not stoichiometric TiO_2, and the atomic ratio of Ti/O is about 1:1.4; there are 6 oxygen vacancies in 10 TiO_2 molecules as reflected by EDS analysis (Figure S1 in the Supporting Information). The existence of oxygen vacancies and Ti ions with valence less than four resulted mainly from incomplete oxidation during rapid quenching and transient reaction.[22,25] In addition, the zeta potential of the TiO_x colloids was approximately −45.4 mV by Gauss Fitting (see Figure S2 in the Supporting Information), indicating that surfaces of the species in the colloid are negatively charged. When the $AgNO_3$ solution was added dropwise and ultrasonically dispersed, the positively charged Ag^+ ions could be easily absorbed on the negatively charged surfaces. After hydrothermal treatment, these colloidal species will grow into nanocrystals through oriented aggregation and Oswald ripening,[26,27] which was confirmed by our earlier work.[23,28] In this process, many oxygen vacancies and surface defects could disappear, accompanied by the release of electrons, which can reduce the absorbed Ag^+ ions. The reaction process can be described as follows:

$$Ti^{(4-x)+} - xe^- = Ti^{4+} \ (x \approx 1.4)$$

$$Ag^+ + e^- = Ag$$

Finally, Ag clusters would be uniformly loaded onto the surface of TiO_2 NPs.

XRD Analysis of Ag/TiO_2 NPs. The X-ray diffraction patterns of the as-synthesized TiO_2 and Ag/TiO_2 NPs samples are shown in Figure 1. The peaks located at 2θ values of 38.1, 44.3, 64.4, and 77.4 can be indexed to (111), (200), (220), and (311) diffractions of cubic structured Ag with lattice constant a = 4.0861 Å (JCPDS no. 65-2871). Those peaks located at 2θ values 25.2, 38.6, 48.1, 53.8, 55.1, 62.6, 68.8, 70.2, and 75.0 can respectively be assigned to (101), (112), (200), (105), (211), (204), (116), (220), and (215) diffractions of anatase phase of TiO_2 (JCPDS no. 21-1272). The existence of the diffraction peaks from Ag and TiO_2 suggests the synthesized samples are composed of both phases. The broadened diffraction peaks indicate the sizes of the Ag/TiO_2 NPs are very small. When the

dx.doi.org/10.1021/la2043526 | Langmuir 2012, 28, 3938−3944

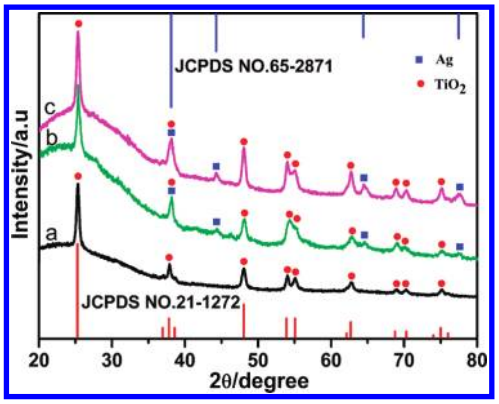

Figure 1. XRD spectra of the as-synthesized TiO_2 (a), 0.54 atom % Ag/TiO_2 NPs (b), and 1.08 atom % Ag/TiO_2 NPs (c).

silver ion concentration was adjusted to 5 μM (0.54 atom % Ag/TiO_2), the intensity of the broadened Ag diffraction peaks weakened, suggesting that the amount of doped Ag was not large and the sizes of Ag NPs were very small (blue mark in Figure 1b). Comparatively, when the silver ion concentration was tuned to 10 μM (1.08 atom % Ag/TiO_2), the Ag diffraction peaks (Figure 1c) became much clearer, indicating that much more Ag NPs were doped. This was confirmed by the following TEM investigations.

Optical Absorption of Ag/TiO_2 NPs. The UV−vis spectra shown in Figure 2a indicate the substantial difference in absorption behavior of TiO_x colloids at room temperature (curve A), TiO_2 NPs (curve B), 0.54 atom % Ag/TiO_2 NPs (curve C), and 1.08 atom % Ag/TiO_2 NPs (curve D). In the absorption spectra of samples C and D, there are no characteristic surface plasmon resonance peaks of Ag around 420 nm; there is a very weak peak at approximately 340 nm, which could be attributed to the less than 5 nm Ag clusters with strong quantum confinement effects,[29] simultaneously demonstrating that no large Ag NPs exist in samples C and D. Based on the diffuse reflectance spectra, the Kubelka−Munk method was used to determine the band gap of the nanocrystals.[30] For the direct band gap semiconductor, the relation between absorption coefficient (α) and photon energy ($h\nu$) can be written as follows:

$$\alpha = B_d(h\nu - E_g)^{1/2}/h\nu$$

where B_d is the absorption constant for direct transition. α can be obtained by the scattering and reflectance spectra on the basis of Kubelka−Munk theory.[31] In addition, the band gap energy value of TiO_2 modified with Ag NPs could also be determined based on the Kubelka−Munk function.[32] Plots of the $(\alpha h\nu)^2$ versus photon energy ($h\nu$) are shown in Figure 2b. The direct band gap energies evaluated from the intercept of the tangents to the plots are 3.40, 3.23, 3.12, and 3.06 eV, corresponding to samples A, B, C, and D. Evidently, through hydrothermal treatment-induced crystallization together with doping of Ag clusters, the band gap energies of samples could be varied. Simultaneously, the absorption area of TiO_2 with doping of Ag clusters was extended to about 410 nm, accompanying a color change in the colloid from blue to brown (see inset of Figure 2a).

TEM-EDS Analysis of Ag/TiO_2 NPs. TEM combined with an energy dispersive spectroscopy (EDS) probe can simultaneously analyze the morphology and microscopic elements of the product. Before taking the TEM images, it is necessary to first collect the EDS spectrum, thus avoiding any change of fine NPs induced by high-energy electron beam irradiation. Comparing EDS spectra (Figure 3g, h) of the samples with and without addition of silver ions, Ag characteristic peaks located ~3 keV are clearly seen. The copper and carbon signals originate from the carbon-coated copper grid. From the EDS spectrum of Ag/TiO_2 NPs with 5 μM $AgNO_3$, the atomic ratio of Ag to Ti was estimated to be about 0.45%. In Figure 3a, b, TEM and HRTEM images for the pure anatase NPs show a mean size of ~23 nm and well crystallinity. In Ag cluster-doped TiO_2 NPs from sample C (0.54 atom % Ag/TiO_2 NPs), many ultrafine black dots in contrast are displayed (Figure 3c); the HRTEM image further demonstrates these dots are Ag clusters, which disperse uniformly over the large anatase NPs, as shown in Figure 3d. The Ag clusters have a mean size of ~3 nm and a narrow size distribution. Subject to identical hydrothermal conditions with 10 μM $AgNO_3$, the Ag clusters (~5 nm) remain highly dispersed and with narrow size distribution over the TiO_2 nanoparticle surfaces (Figure 3e). The maximum concentration of silver ion reduced and uniformly doped is about 15 μM to the colloid prepared in this condition. If the silver ion concentration were to be increased to 20 μM without changing other parameters, the Ag/TiO_2 composite would contain larger Ag particles (5−25 nm) in a wide size distribution (see Figure S3 in the Supporting Information). Apparently, the size and distribution of doped Ag clusters can

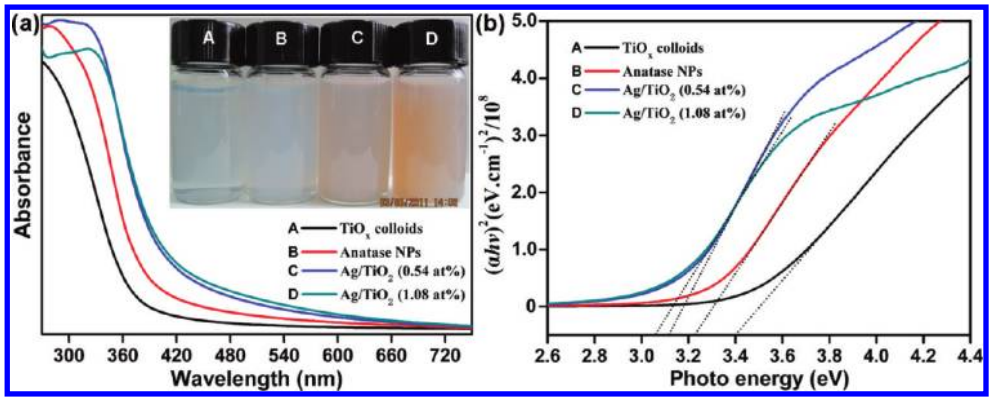

Figure 2. (a) UV−vis absorption spectra of the synthesized samples (inset shows the colloidal color changes) and (b) plots $(\alpha h\nu)^2$ versus $h\nu$ plots for band gap energies.

dx.doi.org/10.1021/la2043526 | Langmuir 2012, 28, 3938−3944

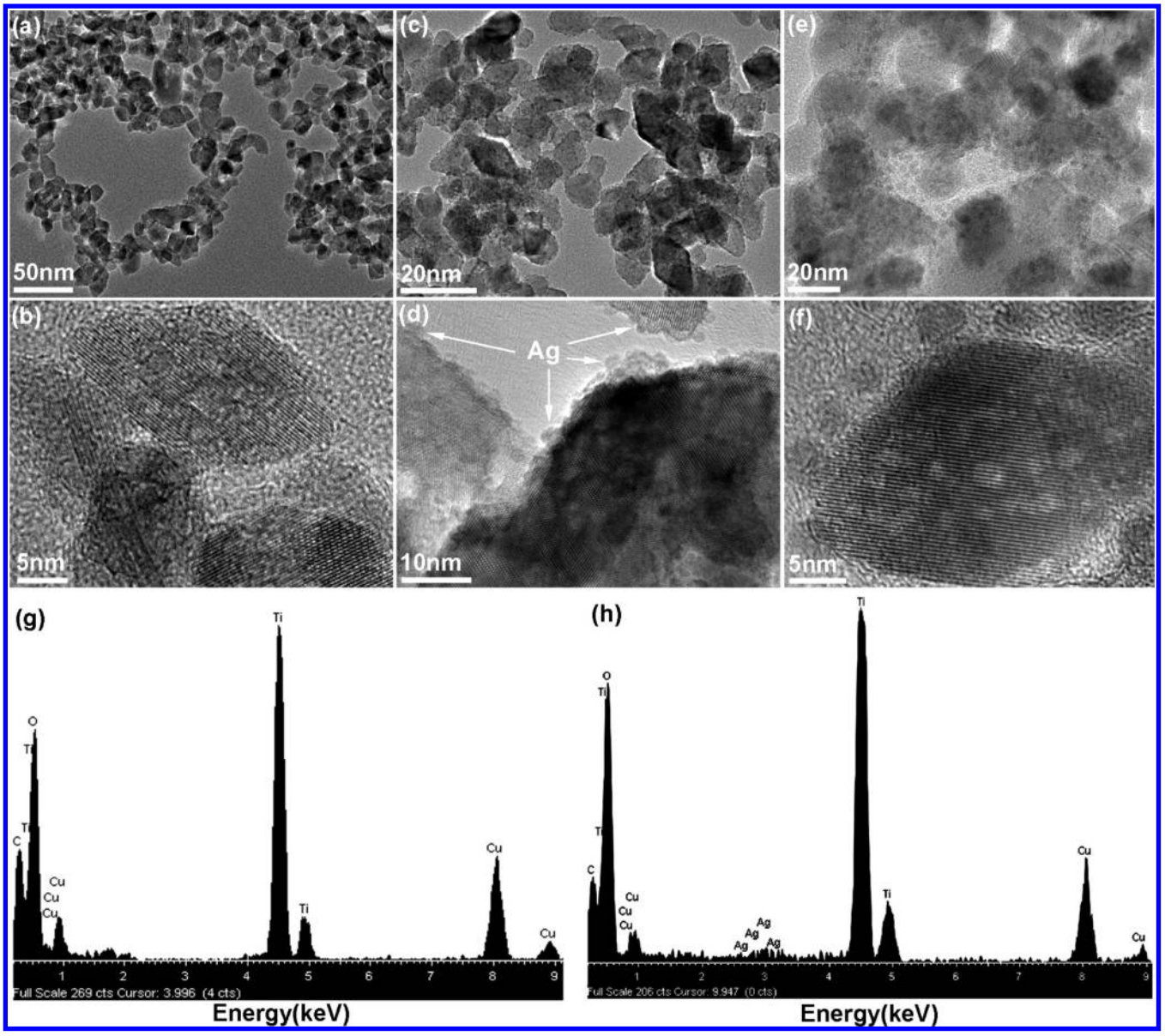

Figure 3. TEM-EDS results: (a, b) without $AgNO_3$, (c, d) with 5 μM $AgNO_3$, (e, f) with 10 μM $AgNO_3$; (g) EDS image of (a), and (h) EDS image of (c).

be tuned by adjusting the $AgNO_3$ concentration. In order to figure out the final conversion of Ag ions into Ag clusters, we tested the upper transparent solution of the 1.08 atom % sample (10 μM $AgNO_3$) using ICP-AES, indicating that the residual concentration of silver ions was about 995.7 ppm (part per million). Comparatively, the initial concentration of silver ions was about 1078.7 ppm. Therefore, the conversion efficiency of Ag ions could reach up to approximately 7.7%.

Valence State of Ag NPs. Although EDS probing has effectively confirmed the existence of Ag element, it cannot distinguish the valence states of the elements. In order to reveal the Ag valence states (oxidized or metallic), XPS spectra of Ag/TiO_2 NPs were measured. The relative peak shifts from the electrostatic charge-up were calibrated using C1s peak at 284.6 eV. The full XPS spectrum of Ag/TiO_2 NPs from sample C (0.54 atom % Ag/TiO_2 NPs) is shown in Figure 4a (spectra from another sample was similar). Ti, Ag, O, and C elements are clearly indicated, with sharp photoelectron peaks at binding energies of 530 eV (O1s), 459 eV (Ti2p), 368 eV (Ag3d), and 285 eV (C1s). Although silver ion concentration is low (5 μM), the signal from the Ag3d states is obvious, indicating Ag clusters are largely dispersed onto the surfaces of anatase NPs, in accordance with the above TEM observation. The XPS spectrum confined to the Ag window (Figure 4c) presents the binding energies of the $Ag3d^{5}/_{2}$ and $Ag3d^{3}/_{2}$ peaks corresponding to 368.1 and 374.1 eV, respectively. Therefore, the Ag clusters exist predominantly in metallic form.[33] The gap of 6.0 eV between the two states is also indicative of metallic Ag.[34] These results are in accordance with the above XRD analysis. As shown in Figure 4b, binding energies of 458.7 and 464.4 eV corresponding to the peaks of $Ti2p^{3}/_{2}$ and $Ti2p^{1}/_{2}$, and the 5.7 eV gap between two states are attributed to the lattice of Ti in TiO_2 with 2p3 binding energy of the Ti(IV) ion.[35]

From high-resolution spectra of Ti2p and Ag3d, the element ratio of Ag to Ti was evaluated about 0.87%. There is a relative discrepancy between EDS and XPS characterization results due to the instrument errors. Results from deconvolution of the

dx.doi.org/10.1021/la2043526 | Langmuir 2012, 28, 3938−3944

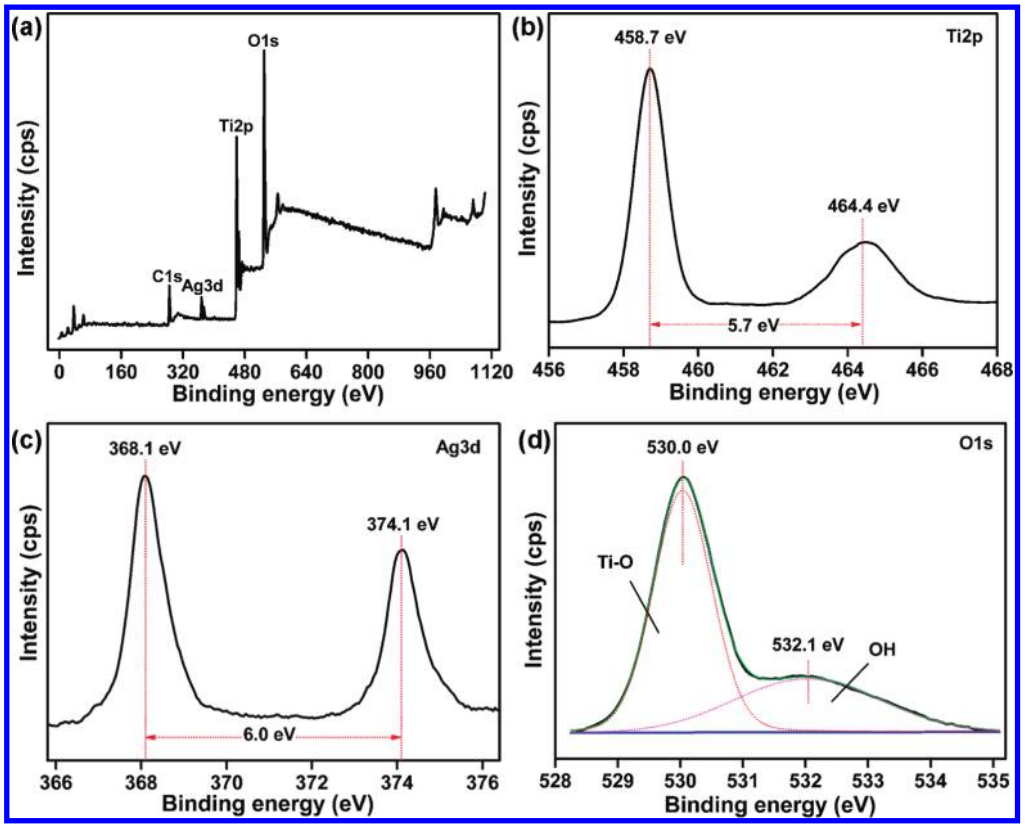

Figure 4. XPS analysis results of 0.54 atom % Ag/TiO_2 NPs: the full XPS spectrum (a) and high-resolution spectra of Ti2p (b), Ag3d (c), and O1s (d) states, respectively.

O1s XPS spectrum suggest oxygen has two peaks at 530.0 and 532.1 eV that are ascribed to Ti−O in TiO_2 and the OH on the surface of TiO_2.[36] The hydroxyl on the surface could be formed during the hydrothermal treatment and preparation of the XPS samples.

Photocatalytic Degradation Properties. The photocatalytic degradation of PCP in aqueous solution using different samples was carried out as shown in Figure 5. Obviously, the efficiency of the TiO_2 catalysts can be improved with the doped Ag clusters. The sample of TiO_x produced by LAL as the catalyst, about 60% PCP could be degraded in 160 min (Figure 5a), which was probably attributed to its wide band gap energy (3.4 eV). Using TiO_2 NPs synthesized without addition of silver ions, about 70% PCP can be decomposed in 160 min (Figure 5b), whereas using 0.54 atom % and 1.08 atom % Ag/TiO_2 catalysts increase the degradation rate to approximately 90% (Figure 5c) and almost 98% (Figure 5d) during the same time, respectively. Compared with TiO_2 without Ag clusters decoration, the catalytic efficiency for PCP was improved about 30% with Ag-doped TiO_2 in 160 min. In the initial 40 min, the PCP concentrations of all chambers with different catalysts deceased rapidly, which was probably related to dechlorination of PCP after adsorption−desorption equilibrium under the ultraviolet light irradiation.[37] Subsequently, the reaction profiles for all samples by and large followed the first-order kinetic (see Figure S4 in the Supporting Information), which was consistent with previous results.[38,39]

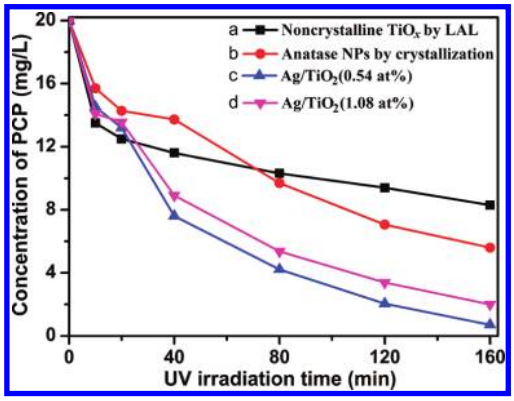

Figure 5. Degradation curves of PCP over noncrystalline TiO_x by LAL (a), anatase TiO_2 NPs by crystallization (b), 0.54 atom % Ag/TiO_2 NPs (c), and 1.08 atom % Ag/TiO_2 NPs (d).

The results suggest the photocatalytic activities of TiO_2 with Ag clusters deposited were enhanced remarkably. Certainly, there was an optimum amount of the silver.[32] If the amount of Ag loaded was excessively large, the metal would rapidly become the recombined center of the electron−hole pairs. It is commonly known that under UV-light excitation, the electrons of the TiO_2 valence band are excited to the conductor band. When loading the Ag NPs on the surface of TiO_2, Ag and TiO_2 form a heterojunction (Schottky junction) where conduction band electrons are transferred to the Ag clusters because of silver's higher work function, thus effectively blocking the recombination of hole−electron pairs.[40−42] The schematic illustration for charge separation of Ag/TiO_2 NPs was shown in Scheme 2. Recently, Ingram et al.[43] demonstrated that plasmonic nanostructures (for example Ag and Au) support the formation of resonant surface plasmons in response to a photon flux, allowing for the selective formation of electron−hole pairs in the near-surface region of the semiconductor,

dx.doi.org/10.1021/la2043526 | Langmuir 2012, 28, 3938−3944

Scheme 2. Schematic Illustration for Charge Separation of Ag/TiO_2 NPs

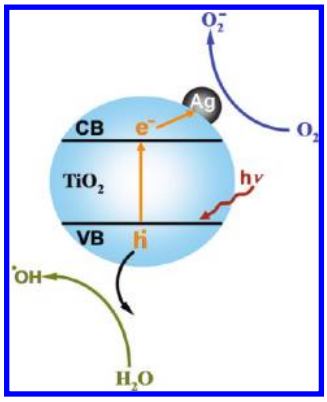

which could readily separated these carriers from each other and easily migrate to the surface, where they can carry out photocatalytic performance. Consequently, electrons on the Ag/TiO_2 composite surface are scavenged by the existing molecular oxygen to produce reactive oxygen radicals (O_2^-), resulting in strong photocatalytic activities, whereas the valence band holes reacted with absorbed surface OH^- group and/or H_2O molecules to form hydroxyl radicals (·OH) possessing high oxidizability.[44,45] The generated strong oxidizing hydroxyl radicals may, in turn, attack organic contaminants like PCP. Furthermore, the existence of plasmonic nanostructures in response to a photon flux ultimately yielded a high concentration of TiO_2 e^-/h^+ pairs in the Ag/TiO_2 nanocomposite compared to the TiO_2-only samples.[46] Therefore, the TiO_2 photocatalysts with the doped Ag clusters exhibited enhanced performance.

In order to evaluate the photocatalytic properties of Ag/TiO_2 prepared by our strategy, the nanocomposite of Ag/TiO_2 by other methods was roughly contrasted. For example, the 1.0% Ag/TiO_2 nanocomposite (10 mg) synthesized by the conventional method could degrade about 22% methylene blue dye (10 mL, 30 μM) in 90 min, while the 1.0% Ag/TiO_2 after calcination could degrade about 58% under identical conditions.[47] Comparatively, the 1.08 atom % Ag/TiO_2 (2.5 mg) prepared by our strategy could decompose about 80% PCP (20 mL, 20 mg/L) in 90 min. Taken as a whole, the latter should have better photocatalytic property. The reasons could be attributed to the following aspects. First, based on LAL technique and hydrothermal treatment, about 25 nm Ag/TiO_2 nanocomposites are successfully synthesized with narrow size distribution. Besides, the Ag clusters are less than 5 nm in size possessing highly dispersed. Furthermore, the combination between Ag clusters and TiO_2 NPs would be stronger than that synthesized by conventional methods, because silver ions were reduced in situ in the crystallization process of TiO_x species and loaded onto the surface of TiO_2 NPs finally formed. Therefore, it is expected that the prepared Ag/TiO_2 nanocomposite using this strategy should possess better photocatalytic performance than that using the conventional methods because of the synthesized process without any organic ligands (including stabilizer and dispersant agents), which seriously resulted in significant blockage of active sites on the surface of Ag/TiO_2 nanocomposite, and consequently influenced their catalytic activities.

CONCLUSIONS

We developed a novel strategy to prepare composited Ag/TiO_2 NPs in narrow size distribution without using any chemical reducing agent and/or organic additive. Ag clusters smaller than 5 nm were uniformly deposited onto TiO_2 NPs. Different from other techniques, the Ag^+ ions were reduced and grown on the surface of anatase NPs, followed by the removal of oxygen vacancies and further oxidation of less valent $Ti^{n+}(n < 4)$ ions. Simultaneously, amorphous-like TiO_x species evolved into well-crystallized TiO_2 nanocrystallites. XRD and XPS analysis results suggested the Ag existed mainly in metallic form. The absorption peak of initial LAL-derived TiO_x colloids is red-shifted after Ag cluster doping, indicating the possible utilization of visible light. The tested photocatalytic properties demonstrated the efficiency of the photocatalysts was largely improved with Ag cluster-doped TiO_2.

This method is simple and effective, simultaneously having a certain universality, which can be extended to prepare other noble metal/semiconductor composites, such as Si, Ge, Sn colloids, and other noble metal ions (Au and Pt).

ASSOCIATED CONTENT

Supporting Information

Additional EDX analysis (Figure S1) of species induced by LAL technique, zeta potential (Figure S2), TEM image and corresponding XRD spectrum (Figure S3), and plots by taking a logarithm of PCP concentrations as a function of time (Figure S4). This material is available free of charge via the Internet at http://pubs.acs.org.

AUTHOR INFORMATION

Corresponding Author

*Phone: +86-551-5591129. Fax: +86-551-5591434. E-mail: chliang@issp.ac.cn.

Notes

The authors declare no competing financial interest.

ACKNOWLEDGMENTS

This work was financially supported by the National Natural Science Foundation of China (grant no. 10974204, 50931002) and Hundred Talent Program of Chinese Academy of Sciences.

REFERENCES

(1) Matthey, D.; Wang, J. G.; Wendt, S.; Matthiesen, J.; Schaub, R.; Laegsgaard, E.; Hammer, B.; Besenbacher, F. *Science* **2007**, *315*, 1692–1696.
(2) Jakob, M.; Levanon, H.; Kamat, P. V. *Nano Lett.* **2003**, *3*, 353–358.
(3) Chen, M.; Goodman, D. W. *Chem. Soc. Rev.* **2008**, *37*, 1860–1870.
(4) Subramanian, V.; Wolf, E. E.; Kamat, P. V. *J. Am. Chem. Soc.* **2004**, *126*, 4943–4950.
(5) Corma, A.; Serna, P.; García, H. *J. Am. Chem. Soc.* **2007**, *129*, 6358–6359.
(6) Turner, M.; Golovko, V. B.; Vaughan, O. P. H; Abdulkin, P.; Berenguer-Murcia, A.; Tikhov, M. S.; Johnson, B. F. G.; Lambert, R. M. *Nature* **2008**, *454*, 981–983.
(7) Subramanian, V.; Wolf, E. E.; Kamat, P. V. *J. Phys. Chem. B* **2003**, *107*, 7479–7485.
(8) Hirakawa, T.; Kamat, P. V. *J. Am. Chem. Soc.* **2005**, *127*, 3928–3934.
(9) Hagfeldt, A.; Graetzel, M. *Chem. Rev.* **1995**, *95*, 49–68.
(10) Zhang, H. J.; Chen, G. H. *Environ. Sci. Technol.* **2009**, *43*, 2905–2910.

(11) Menéndez-Flores, V. M.; Friedmann, D.; Bahnemann, D. W. *Int. J. Photoenergy* **2008**, *2008*, 280513.
(12) Tada, H.; Ishida, T.; Takao, A.; Ito, S. *Langmuir* **2004**, *20*, 7898−7900.
(13) Morones, J. R.; Elechiguerra, J. L.; Camacho, A.; Holt, K.; Kouri, J. B.; Ramirez, J. T.; Yacaman, M. J. *Nanotechnology* **2005**, *16*, 2346−2353.
(14) Zheng, J.; Dickson, R. M. *J. Am. Chem. Soc.* **2002**, *124*, 13982−13983.
(15) Gogoi, S. K.; Gopinath, P.; Paul, A.; Ramesh, A.; Ghosh, S. S.; Chattopadhyay, A. *Langmuir* **2006**, *22*, 9322−9328.
(16) Kong, H.; Jang, J. *Langmuir* **2008**, *24*, 2051−2056.
(17) Wodka, D.; Bielanska, E.; Socha, R. P.; Elzbieciak-Wodka, M.; Gurgul, J.; Nowak, P.; Warszynski, P.; Kumakiri, I. *ACS Appl. Mater. Interfaces* **2010**, *2*, 1945−1953.
(18) Cozzoli, P. D.; Comparelli, R.; Fanizza, E.; Curri, M. L.; Agostiano, A.; Laub, D. *J. Am. Chem. Soc.* **2004**, *126*, 3868−3879.
(19) Pillai, Z. S.; Kamat, P. V. *J. Phys. Chem. B* **2003**, *108*, 945−951.
(20) Li, Y.; El-Sayed, M. A. *J. Phys. Chem. B* **2001**, *105*, 8938−8943.
(21) Narayanan, R.; El-Sayed, M. A. *J. Am. Chem. Soc.* **2003**, *125*, 8340−8347.
(22) Liang, C. H.; Shimizu, Y.; Sasaki, T.; Koshizaki, N. *J. Phys. Chem. B* **2003**, *107*, 9220−9225.
(23) Zhang, H. M.; Liang, C. H.; Tian, Z. F.; Wang, G. Z.; Cai, W. P. *CrystEngComm* **2011**, *13*, 4676−4682.
(24) Zhang, H. M.; Liang, C. H.; Tian, Z. F.; Wang, G. Z.; Cai, W. P. *J. Phys. Chem. C* **2010**, *114*, 12524−12528.
(25) Liang, C. H.; Shimizu, Y.; Sasaki, T.; Koshizaki, N. *Appl. Phys. A: Mater. Sci. Process* **2005**, *80*, 819−822.
(26) Penn, R. L.; Banfield, J. F. *Science* **1998**, *281*, 969−971.
(27) Zhang, J.; Huang, F.; Lin, Z. *Nanoscale* **2010**, *2*, 18−34.
(28) Zhang, H. M.; Liang, C. H.; Tian, Z. F.; Wang, G. Z.; Cai, W. P. *CrystEngComm* **2011**, *13*, 1063−1066.
(29) Ganeev, R. A.; Suzuki, M.; Baba, M.; Ichihara, M.; Kuroda, H. *J. Phys. B: At., Mol. Opt. Phys.* **2008**, *41*, 045603.
(30) Serpone, N.; Lawless, D.; Khairutdinov, R. *J. Phys. Chem.* **1995**, *99*, 16646−16654.
(31) Yu, J. G.; Xiang, Q. J.; Zhou, M. H. *Appl. Catal., B* **2009**, *90*, 595−602.
(32) Wodka, D.; Bielanska, E.; Socha, R. P.; Elzbieciak-Wodka, M.; Gurgul, J.; Nowak, P.; Warszynski, P.; Kumakiri, I. *ACS Appl. Mater. Interfaces* **2010**, *2*, 1945−1953.
(33) Moulder, J. F.; Stickle, W. F.; Sobol, P. E.; Bomben, K. D. *Handbook of X-ray Photoelectron Spectroscopy: A Reference Book of Standard Spectra for Identification and Interpretation of XPS Data*; Physical Electronics Division, Perkin-Elmer Corp.: Eden Prairie, MN, 1992.
(34) Niemantsverdriet, J. W. *Spectroscopy in Catalysis: An Introduction*; Wiley-VCH: Weinheim, Germany, 2000.
(35) Sanjines, R.; Tang, H.; Berger, H.; Gozzo, F.; Margaritondo, G.; Levy, F. *J. Appl. Phys.* **1994**, *75*, 2945−2951.
(36) Yu, J. G.; Yu, H. G.; Cheng, B.; Zhou, M. H.; Zhao, X. J. *J. Mol. Catal. A: Chem.* **2006**, *253*, 112−118.
(37) Suegara, J.; Lee, B. D.; Espino, M. P.; Nakai, S.; Hosomi, M. *Chemosphere* **2005**, *61*, 341−346.
(38) Pecchi, G.; Reyes, P.; Sanhueza, P.; Villaseñor, J. *Chemosphere* **2001**, *43*, 141−146.
(39) Villaseñor, J.; Reyes, P.; Pecchi, G. *J. Chem. Technol. Biotechnol.* **1998**, *72*, 105−110.
(40) He, X. L.; Cai, Y. Y.; Zhang, H. M.; Liang, C. H. *J. Mater. Chem.* **2011**, *21*, 475−480.
(41) Wold, A. *Chem. Mater.* **1993**, *5*, 280−283.
(42) Linsebigler, A. L.; Lu, G. Q.; Yates, J. T. *Chem. Rev.* **1995**, *95*, 735−758.
(43) Ingram, D. B.; Linic, S. *J. Am. Chem. Soc.* **2011**, *133*, 5202−5205.
(44) Arabatzis, I. M.; Stergiopoulos, T.; Bernard, M. C.; Labou, D.; Neophytides, S. G.; Falaras, P. *Appl. Catal., B* **2003**, *42*, 187−201.
(45) Liu, S. X.; Qu, Z. P.; Han, X. W.; Sun, C. L. *Catal. Today* **2004**, *93*−*95*, 877−884.
(46) Christopher, P.; Ingram, D. B.; Linic, S. *J. Phys. Chem. C* **2010**, *114*, 9173−9177.
(47) Wang, J. Y.; Zhao, H. T.; Liu, X. R.; Li, X. D.; Xu, P.; Han, X. J. *Catal. Commun.* **2009**, *10*, 1052−1056.